ACS APPLIED MATERIALS & INTERFACES

Research Article

Cite This: ACS Appl. Mater. Interfaces 2018, 10, 4530−4539

www.acsami.org

Coordination-Triggered Hierarchical Folate/Zinc Supramolecular Hydrogels Leading to Printable Biomaterials

Kaerdun Liu,[†] Shihao Zang,[†] Rongrong Xue,[†] Jinghui Yang,[‡] Lizhi Wang,[‡] Jianbin Huang,[†] and Yun Yan*[,†]

[†]Beijing National Laboratory for Molecular Sciences (BNLMS), State Key Laboratory for Structural Chemistry of Unstable and Stable Species, College of Chemistry and Molecular Engineering, Peking University, Beijing 100871, P. R. China

[‡]College of Chemistry and Chemical Engineering, Xinjiang University, Urumqi 830046, P. R. China

Supporting Information

ABSTRACT: Printable hydrogels desired in bioengineering have extremely high demands on biocompatibility and mechanic strength, which can hardly be achieved in conventional hydrogels made with biopolymers. Here, we show that on employment of the strategy of coordination-triggered hierarchical self-assembly of naturally occurring small-molecule folic acid, supramolecular hydrogels with robust mechanical elastic modulus comparable to synthetic double-network polymer gels can be made at concentrations below 1%. A sequence of hierarchical steps are involved in the formation of this extraordinary hydrogel: petrin rings on folate form tetramers through hydrogen bonding, tetramers stack into nanofibers by $\pi-\pi$ stacking, and zinc ions cross-link the nanofibers into larger-scale fibrils and further cross-link the fibril network to gel water. These supramolecular qualities endow the hydrogel with shear-thinning and instant healing ability, which makes the robust gel injectable and printable into various three-dimensional structures. Owing to the excellent biocompatibility, the gel can support cells three-dimensionally and can be used as an ideal carrier for imaging agent (Gd^{3+}), as well as chemodrugs. In combination with its easy formation and abundant sources, this newly discovered metallo-folate supramolecular hydrogel is promising in various bioengineering technological applications.

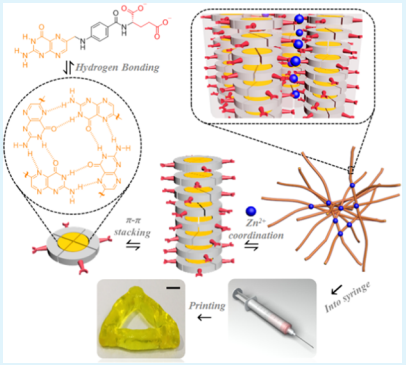

KEYWORDS: *hierarchical assembly, coordination, folic acid, injectable hydrogels, bioprinting*

1. INTRODUCTION

Printable hydrogels are attractive in a number of vital fields, especially as cell-bearing scaffolds in tissue engineering[1−3] and as drug-bearing matrices in delivery system.[4−7] One of the critical requirements for such hydrogels is their biocompatibility. Therefore, a variety of naturally occurring molecules, especially proteins like elastin, collagen, gelatin, and silk fibroin, are of great interest in this field.[8−13] Fibrils can be formed by these molecules, which gel water through formation of three-dimensional (3D) networks.[14−16] However, the hydrogels formed by the family of proteins often have poor mechanical properties, underlying their potential ability as printable materials. The reason is that the physical network of the fibrils is not strong enough to counterbalance the external mechanical stimulus, so that the printability of these hydrogels is not satisfactory. Similar problem exist in hydrogels formed with other biomolecules, including polysaccharides,[17,18] nucleotide,[19] and polyphenol.[20]

To enhance the mechanical properties of hydrogels formed by biomolecules, covalent cross-linking strategy based on chemical reactions is broadly utilized.[21−25] The printable hydrogels require that they should form rapidly, show viscous flow under shear, and rapid recovery (self-healing) after shear (print).[2,26,27] However, cross-linking may result in irreversibility of the flow behavior and the introduction of cross-linking agent will trigger undesired toxicity, dramatically limiting the biomedical application of these hydrogels.

Herein, we propose a coordination-facilitated hierarchical self-assembling and cross-linking pathway for the fabrication of biomolecule-based printable hydrogels with shear-thinning and self-healing properties (Scheme 1). Recently, it was found that coordination between metal ions and biopolymers could be used to construct biocompatible films[28] and healable hydrogels,[20,29−31] where the relatively strong but labile coordination bonds (50−200 kJ mol^{-1} in strength, compared with 5−65 kJ mol^{-1} of hydrogen bonding)[32] are believed to play a key role in cross-linking the biopolymers. Furthermore, the coordination process between metal ions and biopolymers may occur within seconds, which is highly desired in the fabrication of printable hydrogels.[20] Inspired by the elegant approaches achieved in metallo-biopolymer systems, we expected that the coordination-triggered cross-linking of the self-assemblies may allow the generation of robust hierarchical hydrogels that are printable if

Received: November 29, 2017
Accepted: January 16, 2018
Published: January 16, 2018

DOI: 10.1021/acsami.7b18155
ACS Appl. Mater. Interfaces 2018, 10, 4530−4539

Scheme 1. Illustration of the Hierarchical Self-Assembly Process during Gel Formation and the Printed Hollow Triangle Structure[a]

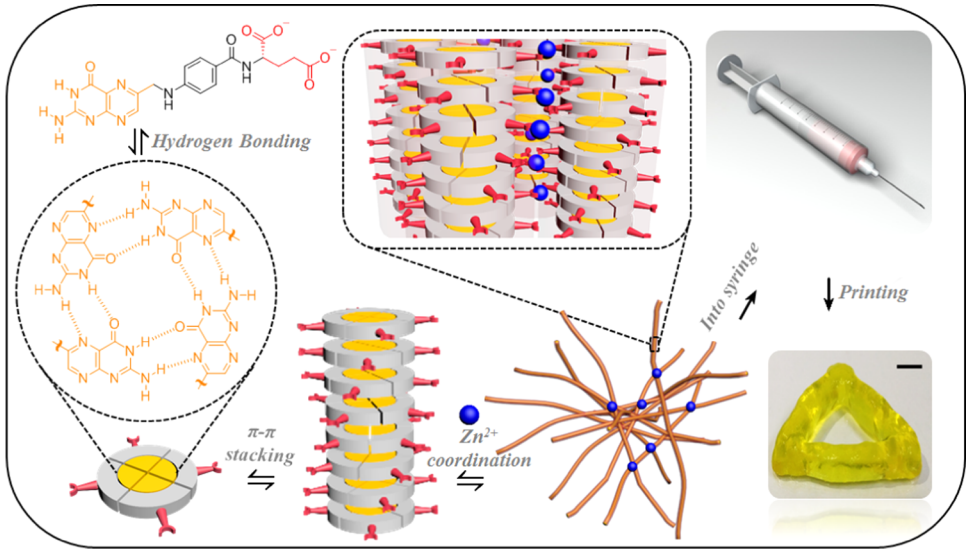

[a]Note: Zn^{2+} cross-links the stacked tetramers into fibrils (which shows in an enlarged image of fibril), and further cross-links the network of the fibrils to form robust hydrogel.

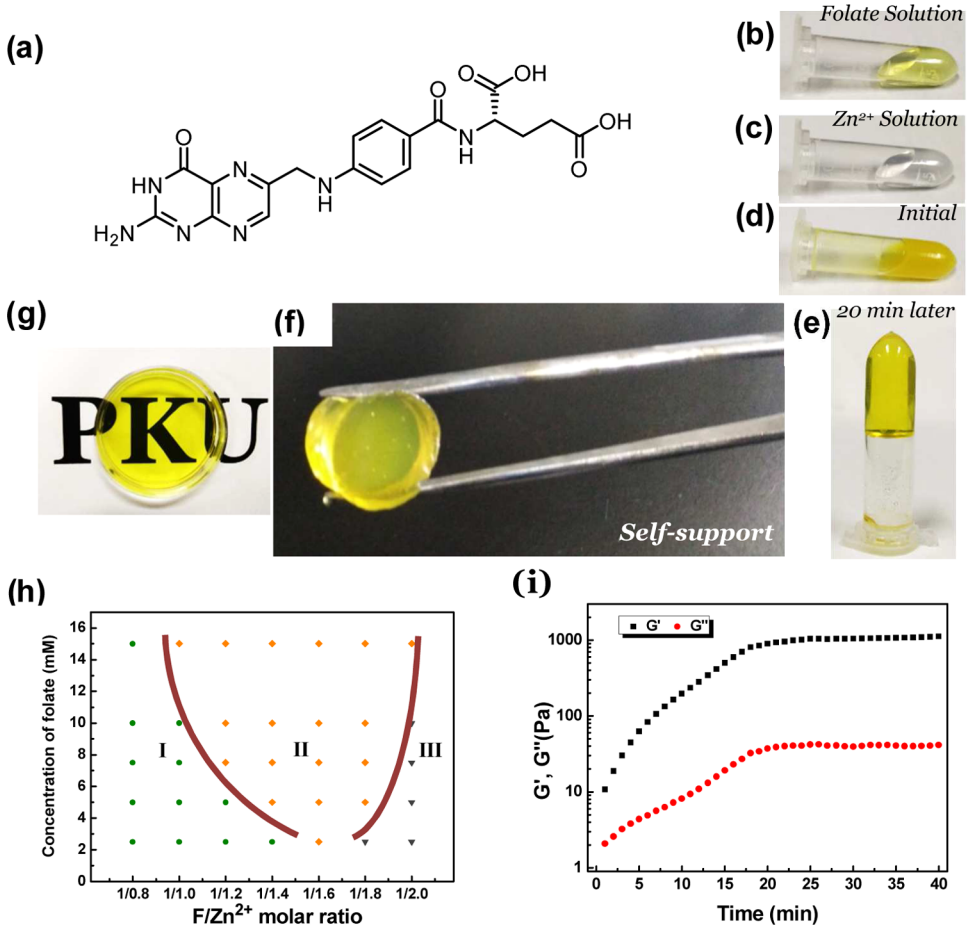

Figure 1. Gelation in the folate/Zn^{2+} system. (a) Structure of folate. Mixing of the folate solution (pH = 11) (b) with $Zn(NO_3)_2$ solution (c) produces an initial viscous system (d), which finally becomes transparent gel (e). (f) Folate/Zn^{2+} gel picked up with tweezers. (g) Folate/Zn^{2+} thin gel prepared on a plastic dish. (h) Phase diagram of folate and Zn^{2+} in water. (i) Dynamic oscillatory rheological measurements showing the gel-formation process of folate/Zn^{2+} system. [Folate] = 15 mM, folate/Zn^{2+} = 1/1.8.

DOI: 10.1021/acsami.7b18155
ACS Appl. Mater. Interfaces 2018, 10, 4530−4539

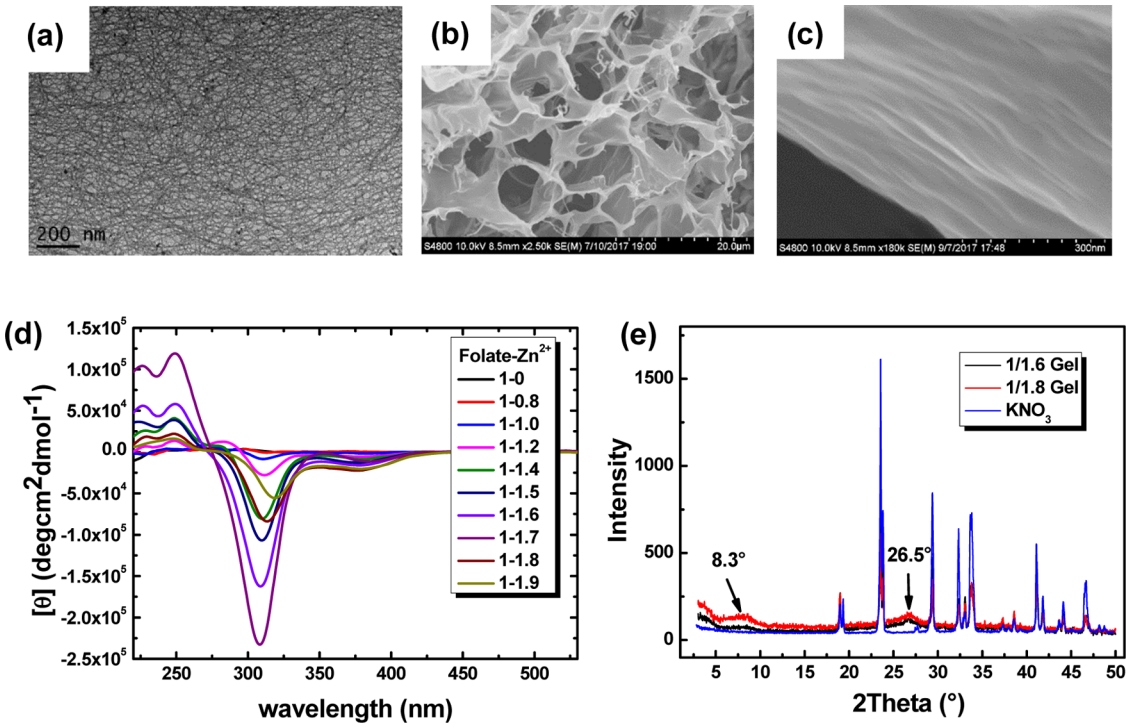

Figure 2. (a) TEM images of folate/Zn^{2+} hydrogel. (b, c) SEM image of lyophilized folate/Zn^{2+} hydrogel. In TEM and SEM observations, [folate] = 15 mM, folate/Zn^{2+} = 1/1.8. (d) Circular dichroism (CD) spectra of folate/Zn^{2+} hydrogel. (e) X-ray diffraction (XRD) patterns of lyophilized folate/Zn^{2+} hydrogel. In CD and XRD measurements, [folate] = 15 mM.

the biopolymers were replaced by the self-assembly of small biomolecules.

Folic acid (Figure 1a) was chosen to construct the coordination-triggered printable hydrogel. As a naturally occuring small molecule, folic acid is essential for human in the synthesis of DNA/RNA and metabolism amino acid.[33−35] The structure of folic acid consists of a pterin ring and a glutamate moiety, which are connected by 4-aminobenzoic acid. The pterin group shows propensity to form a tetramer through hydrogen bonding,[36] which can stack into fibrils and further form liquid crystals in the aqueous solution.[37−39] However, folic acid can only form organogels in dimethyl sulfoxide (DMSO)/water mixed solvent[40,41] owing to its limited water solubility. Here, we bring forward a coordination-triggered metallo-folate supramolecular hydrogel, which is injectable and printable. We first put folic acid in water, followed by increasing the solution pH beyond 10, where folic acid can be solubilized and exists in the form of folate. Amazingly, the solution pH immediately drops back to about 7.0 upon the addition of a range of transition metal ions, and transparent hydrogels are formed. In this work, we show the formation of robust but printable hydrogels with folate and zinc ions as a primary demonstration. (Actually, many other metal ions can also form hydrogel with folate, e.g., nickel ion, magnesium ion, etc.) The gel formation process involves first dissolving folic acid in water at pH > 10 (in basic form as folate), and subsequent addition of $Zn(NO_3)_2$ ions to coordinate with the glutamate group of folate and to bind excess OH^-. Folate at pH > 10 cannot self-assemble into network structures, whereas the addition of Zn^{2+} immediately brings about five important results: (1) enhanced formation of G-tetramers of folate in water; (2) $\pi-\pi$ stacking of the G-tetramers into primary nanofibers; (3) cross-linking of the nanofibers into larger-scale fibrils with Zn^{2+}; (4) formation of the fibrils network to gel water; and (5) spontaneous pH drop to about 7.0 in hydrogel. The resulting hydrogels exhibit advantages as a printable material as well as in vivo injectable material for biomedical applications because of the following reasons: (1) the hydrogels have good biocompatibility and biodegradability because folic acid is a nutrition supplement and Zn is an essential element for humans and other animals, plants, and microorganisms; and (2) the hydrogels allow for flow under applied stress and rapid recovery on the removal of stress, owing to the reversible cross-linking of the folate fibrils with Zn^{2+} ions. Furthermore, the hydrogels can readily sequester magnetic resonance imaging (MRI) agent (Gd^{3+}) or water-soluble drugs, providing a means of imaging and therapy against cancer. Hydrogels subject to intratumoral injection confine drugs in the diseased lesion and provide locally sustained release. Such a delivery vehicle based on folate hydrogels with shear-thinning and self-healing properties can efficiently lower drug dosage to a minimal level, resist clearance of the immune system and, thus to a maximum extent, reduce damage of normal tissues, and finally realizing the purpose of "precise therapy".

2. RESULTS AND DISCUSSION

Folic acid itself cannot form hydrogel in water due to its poor water solubility, but it can form organogel in the mixed solvent of DMSO/water.[40,41] However, we show in Figure 1 that the hydrogels are rapidly formed when a basic folate aqueous solution (15 mM, (0.9% w/w), pH = 11) is mixed with zinc nitrate ($Zn(NO_3)_2$) solution under ambient conditions. The solubility of folate can be enhanced to ∼50 mM in water at a sufficiently high pH. Amazingly, the final pH of the hydrogel drops to ∼7.0 in all of the gels. The gelation can occur at the molar ratios of folate/Zn^{2+} in the range of 1.2−2.0 (Figure 1h for phase diagram). A turbid viscous suspension was formed

DOI: 10.1021/acsami.7b18155
ACS Appl. Mater. Interfaces 2018, 10, 4530−4539

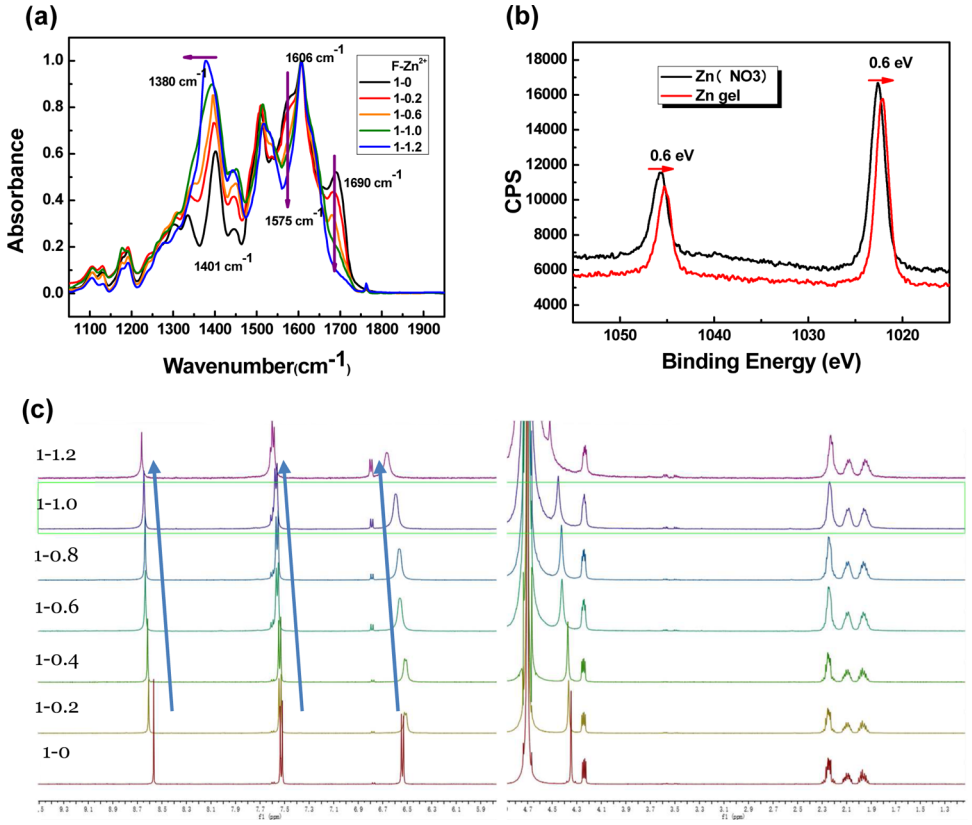

Figure 3. (a) IR spectra of folate/Zn^{2+} hydrogel with increased Zn^{2+}. (b) XPS spectra of lyophilized folate/Zn^{2+} hydrogel (folate/Zn^{2+} = 1/1.8). (c) ^{1}H NMR spectra of folate/Zn^{2+} system with increased folate/Zn^{2+} ratio. [Folate] = 15 mM. The numbers in (c) are the molar ratio between folate and Zn^{2+}.

upon initial mixing, which was then transformed into a transparent hydrogel within ca. 20 min. The obtained hydrogel is optically transparent (Figure 1g), which has enough mechanical strength to support its own weight and retain its shape when picked up with tweezers (Figure 1f).

The gelation process can be monitored with rheological measurements (Figure 1i). Initially, both the storage modulus (G') and the loss modulus (G'') are relatively small, but the G' and G'' increase over time. At about 20 min, G' and G'' reach the stable state, indicating the rapid complement of gel formation. Because the pH of the final hydrogel is around 7.0, it is advantageous for further bioapplication.

Transmission electron microscopy (TEM) images (Figure 2a) reveal that the hydrogels consist of firm and uniform nanofibers that further intertwine into the fibrous scaffold. The fibers are 5−10 nm in width and several micrometer in length. The contrast of these nanofibers is very high without any staining, suggesting the presence of Zn^{2+} inside. Scanning electron microscopy (SEM) observation reveals that the lyophilized gels display a porous structure with the pore size of about 5−10 μm (Figure 2b). Enlarged SEM image shows that the walls of the scaffold are formed with the bundles of nanofibers (Figure 2c).

The nanofibers in the folate−Zn hydrogels are similar to those formed in the organol folate gels.[40,41] Previous study verified that the fibers originate from the stack of the tetramers of folate.[37,38] In this study, the formation of tetramers is confirmed via circular dichromic (CD) and X-ray diffraction (XRD) measurements. The CD spectra of the hydrogels (Figure 2d) display exciton patterns characteristic of a helical arrangement of chromophoric pterin group,[42] which is similar to the CD spectra of folate dipotassium liquid crystal.[37] It is noticed that although folate has a chiral center in glutamate group (Figure 1a), its CD signal is almost completely silent in water in the range of 200−400 nm, ascribed to the pterin ring and benzene ring. Even with the help of KNO_3 (which shows ability to stabilize tetramer structure[38]), the CD signal of folate is still very weak, and the viscosity of the solution is low (Figure S1). This means that the chiral center in glutamic moiety could not be directly transferred to the pterin and benzene rings, or amplified to be detected in the CD spectra without gelation. However, upon gelation triggered by Zn^{2+} coordination, obvious CD signal is observed. The folate/Zn^{2+} gels display the characteristic Cotton effects in the region of 200−400 nm, which are consistent with the absorption band of folate (Figure S2). Especially, the intensity of the CD signal increases with increasing the folate/Zn^{2+} ratio from 1.2 to 1.7, unambiguously confirming that the Zn^{2+}-triggered fiber formation is the origin of the CD signal.

The tetramer formation and its further stacking into fibers are also confirmed with the XRD measurements. In Figure 2e, the lyophilized folate/Zn^{2+} gel shows two peaks at 8.3 and 26.5° apart from sharp peaks from KNO_3 generated by the addition of $Zn(NO_3)_2$ to the basic folate solution. The corresponding distances are 10.7 and 3.36 Å, respectively, whereas the distance of 10.7 Å is close to column diameter of folate tetramers,[37] and the 3.36 Å is a typical distance of $\pi-\pi$ stacking.[37,38,43,44] These two characteristic distances are also observed in situ in the hydrogel with the combination of small angle X-ray scattering and XRD techniques (Figure S3),

DOI: 10.1021/acsami.7b18155
ACS Appl. Mater. Interfaces 2018, 10, 4530−4539

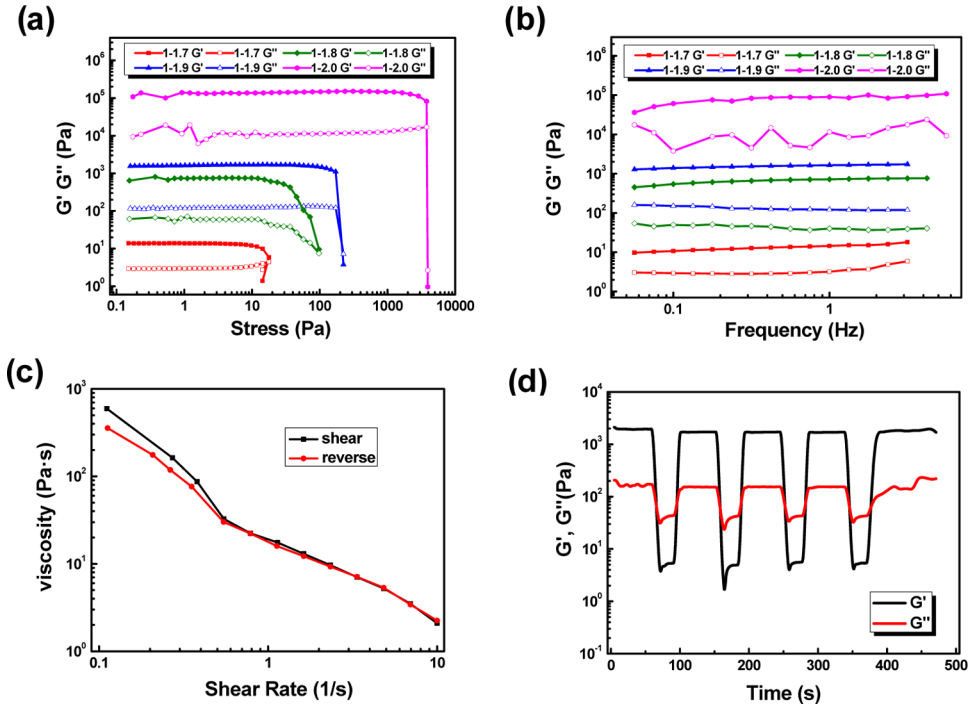

Figure 4. Rheological characterization of injectable folate/Zn^{2+} hydrogels. (a) Stress-dependent (f = 1 Hz), and (b) frequency-dependent (at stress of 1 Pa) oscillatory profiles of folate/Zn^{2+} hydrogel. [Folate] = 15 mM. The numbers in (a) and (b) are the molar ratios between folate and Zn^{2+}. (c) Viscosity of folate/Zn^{2+} hydrogel at increased shear rate followed by reverse shear rate decrease in continuous flow experiments. (d) Continuous step-stain measurements, which were carried out in steps of 50 and 0.5% oscillatory strain for four cycles. (Hydrogels used in (c) and (d) were [folate] = 15 mM, folate/Zn^{2+} = 1/1.8.)

confirming the formation of tetramers and their further $\pi-\pi$ stacking into the nanofibers. It should be pointed out that merely adding KNO_3 to the aqueous solution of folate system cannot generate similar XRD pattern without Zn^{2+}.

To probe the role of Zn^{2+} in the gel formation, Fourier transform infrared measurements were performed. Figure 3a shows that before the addition of Zn^{2+}, the symmetric and asymmetric vibration of the −COO− group occurs at 1401 and 1575 cm^{-1}, respectively, whereas they shift to 1380 and 1606 cm^{-1} upon coordination with Zn^{2+}. This indicates that coordination occurs between the −COO− group and Zn^{2+}. The separation of 1606−1380 cm^{-1} = 226 cm^{-1} suggests a monodendate coordination of Zn^{2+} to the carboxylate group.[45−47] X-ray photoelectron spectroscopy (XPS) in Figure 3b reveals that the coordination results in a decrease in the binding energy of Zn $2p_{1/2}$ and Zn $2p_{3/2}$ by 0.6 eV. Because the −COO− groups are on the periphery of the tetramers that stack into the fibers, it is convincing that Zn^{2+} cross-links the $\pi-\pi$ stacked tetramers into fibrils that are detectable under TEM, whereas the network of the fibrils can be further cross-linked by Zn^{2+}, as illustrated in Scheme 1.

However, the formation of the nanofibers and the coordination with Zn^{2+} occurs simultaneously. The ^1H NMR spectra in Figure 3c show that before the addition of Zn^{2+} to the basic solution of folate, the peaks on the pterin ring occur at δ = 8.57 ppm and on benzene ring at δ = 7.5, 6.53 ppm, respectively. These peaks all shift downfield on addition of $Zn(NO_3)_2$. As the molar ratio of folate/Zn^{2+} increases, the corresponding chemical shifts increase to 8.67 (1H on pterin), 7.59, and 6.66 (2H on benzene), respectively. This means that the stronger deshielding effect on H of pterin ring and benzene ring is a result of increased electron density in the $\pi-\pi$ stacking[48] (Figure 3c). This result also rules out the possibility of the coordination of Zn^{2+} to the N atom in the pterin ring because such a scenario would significantly reduce the electron density on the pterin ring,[49] which is contradiction to the results obtained from the ^1H NMR measurements. Therefore, it is unambiguous that the role of Zn^{2+} in the hydrogel is to cross-link the stacked folate tetramer via coordination interaction into fiber bundles, which finally gels the system.

Printable hydrogel should meet two main requirements: shear-thinning and fast gelation/cross-linking rate. Both of these requirements can be measured by the rheological properties of hydrogel. Figure 4 shows the rheogram for the hydrogels formed with 15 mM (0.9% w/w) folate on increasing molar ratio of folate/Zn^{2+} from 1/1.7 to 1/2.0. First, the frequency sweep results show that both the storage modulus (elastic modulus, G') and the loss modulus (viscous modulus, G'') are basically independent of the frequency (f), whereas G' dominates G'' over the entire investigated frequency range by 1 order (Figure 4b), characterizing a typical solidlike rheological behavior of the hydrogel. Second, both the moduli and the yield point increase with increasing molar ratio of folate/Zn^{2+}. Figure 4a shows that the elastic modulus G' is increased by about 5 orders, namely, from 10 to 10^6 Pa, as the molar ratio increases from 1.7 to 2.0, indicating the huge impact of increased density of cross-linkers on the enhancement of the mechanical property of the hydrogel. The large elastic modulus higher than 10^6 Pa reveals that the hydrogels have an excellent mechanical strength required for printing.[2] Furthermore, the mechanical strength of the hydrogel can be further enhanced by increasing the total concentration of the coordinating system at a given folate/Zn^{2+} ratio. In Figure S4, we show that at the folate/Zn^{2+} ratio of 1.8, the elastic modulus can be enhanced 2 orders as the concentration of folate increases from 10 to 30 mM. Such a variation in the molar ratio and the concentration does not

DOI: 10.1021/acsami.7b18155
ACS Appl. Mater. Interfaces 2018, 10, 4530−4539

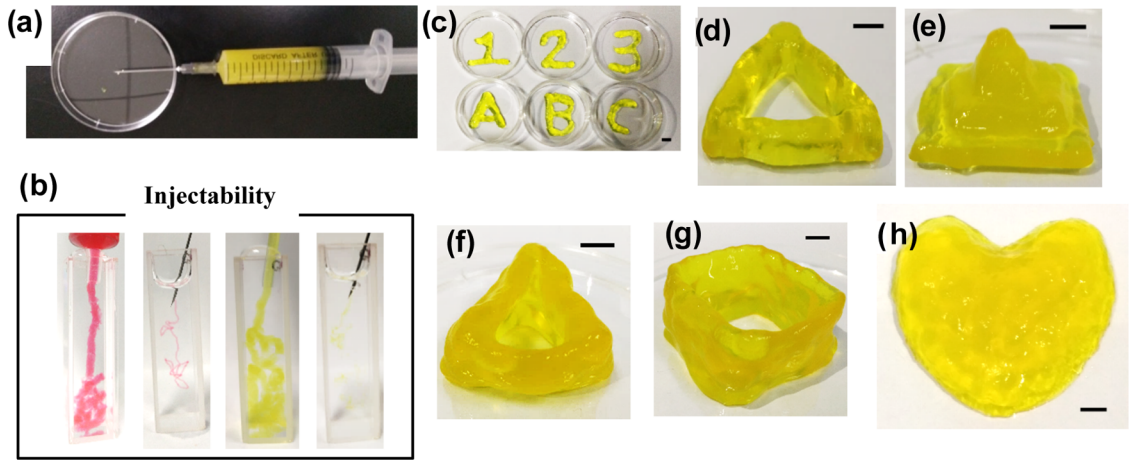

Figure 5. (a) Homemade equipment for gel printing. (b) Injection of folate/Zn^{2+} hydrogel and rhodamine B doped folate/Zn^{2+} hydrogel through narrow and wide needles. Various 3D structures obtained by hydrogel printing: numbers and characters (c), triangle (d), pyramid (e), hollow triangle (f), hollow cube (g), and heart (h). Scale bar = 0.5 cm. [Folate] = 15 mM, folate/Zn^{2+} = 1/1.9.

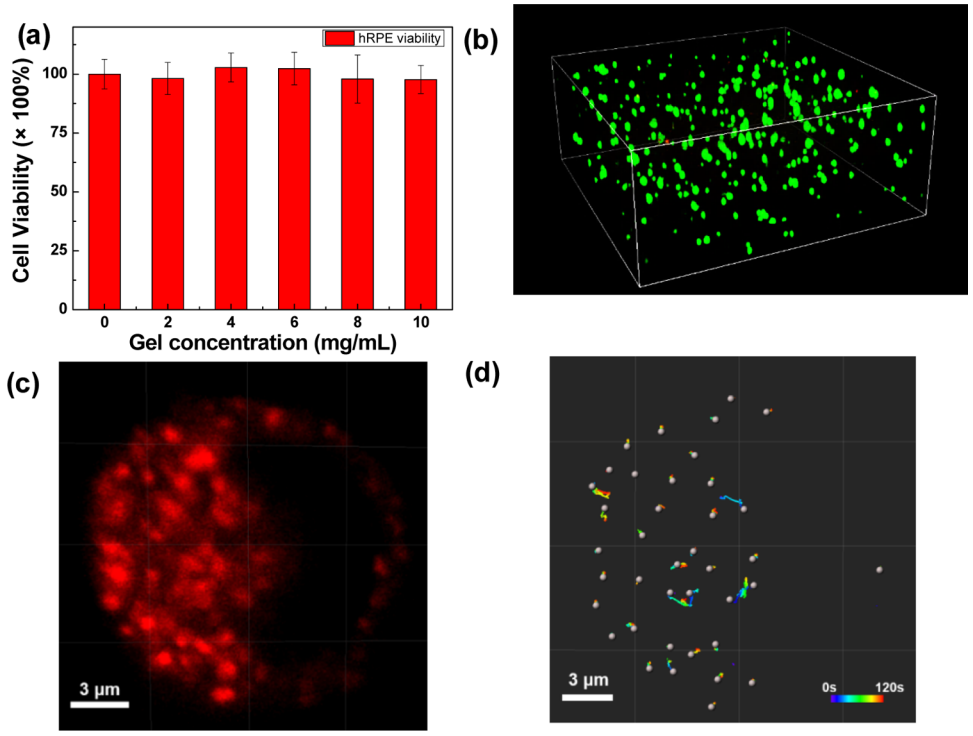

Figure 6. (a) hRPE cell viability printed in the folate/Zn^{2+} hydrogel after 48 h incubation. (b) Three-dimensional stacking confocal laser scanning microscopy (CLSM) image of the hRPE cell embedded in the folate/Zn^{2+} hydrogel with a live/dead assay (1.27 mm in width, 1.27 mm in height, and 0.52 mm in depth). (c) A single hRPE cell was stained by LysoTracker Red showing acidic compartments. (d) Dynamic organelles were tracked, and trajectories from inside the cell are shown in (c). The tracked organelles are shown as gray spheres and the colors of the tracks represent the time (0−120 s). All of the measurements are made after 48 h incubation of the cell in the gel of [folate] = 15 mM, folate/Zn^{2+} = 1/1.8.

affect the printability, indicating the wide capacity of modulating the mechanical strength on the requirements by modifying either the concentration or the molar ratio. It is noticed that the densely cross-linked folate/Zn hydrogel may have an elastic modulus of the same magnitude as the double network (DN) hydrogels of synthetic polymers.[50] The DN hydrogels made with polymers usually display an elastic modulus beyond 10^5 magnitude, which endows them excellent mechanical strength similar to solids.[50] However, the DN gels usually form at very high concentration of polymers and require chemical cross-linking, which makes them absent from the field of printable materials and mainly functioning as solid materials. In contrast, the present folate/Zn^{2+} hydrogels are formed by small molecules driven by reversible noncovalent connections, which endow the robust hydrogel with an excellent shear-responsive flow behavior. The continuous flow experiment in Figure 4c reveals that this robust folate/Zn^{2+} hydrogel still exhibits a good shear-thinning behavior with increasing shear rate from 0.1 to 10 s^{-1}, whereas the viscosity of the hydrogels nearly restores its initial state in the immediately performed reverse cycle. Notice that the recovery process occurs instantly in the reverse cycle, which is even faster than the initial gelation

DOI: 10.1021/acsami.7b18155
ACS Appl. Mater. Interfaces 2018, 10, 4530−4539

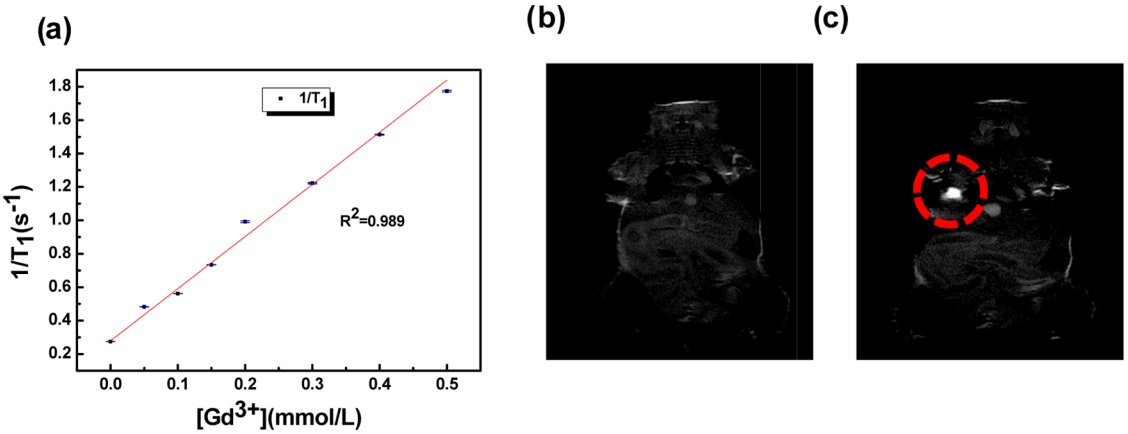

Figure 7. (a) Spin−lattice relaxation time T_1 of the protons in water influenced by Gd^{3+} in folate/Zn^{2+} hydrogels. T_1-weighted MR images of HeLa xenograft nude mice before (b) and after (c) intratumor injection of Gd^{3+}−folate/Zn^{2+} hydrogel. [Folate] = 15 mM, folate/Zn^{2+} = 1/1.8, [Gd^{3+}] = 0.5 mM.

process. From data in Figure 1i, we are able to estimate the gelation rate r in the 15 mM folate system at the folate/Zn^{2+} ratio of 1.8. According to the kink in the $G'-t$ plot, the gelation can be divided into "nucleation stage" (t < 5 min) and "fast gelation stage" (5 min < t < 15 min). The apparent rate r for these two stages can be expressed by two similar exponential equations

$$r = 10^{t/5}\ (t < 5\ \text{min}),\ \text{and}\ r = 10^{t-5/10}\ (5\ \text{min} < t < 15\ \text{min})$$

The exponential rates endow complete gelation within 20 min, but the entire recovery of the gelation state after shear demonstrated in Figure 4c only requires less than 30 s. This result indicates that the shear force only changes the connections between the fibers, so that it is not necessary to reform the gel from the scratch in the recovery process. We assume that the collective $\pi-\pi$ staking between the tetramers affords a robust shear resistance of the fibers, and the reversible coordination between the fibers allows the gel to restructure under shear and to recover rapidly as the shear force is removed.

To provide further convincing evidence of the recovery ability of the folate/Zn^{2+} hydrogel, continuous step change of the oscillatory strain between 50 and 0.5% at the same frequency (1 Hz) is given to assess the strain-induced damage and self-healing property of the hydrogels (Figure 4d). A high-magnitude strain (50%) is applied to break the hydrogel network structure. Following this, a low-magnitude strain (0.5%) is applied to inspect the recovery of the hydrogel structure. Under the small (0.5%) strain, G' is found to be 1 magnitude larger than G'', indicating the existence of the freestanding hydrogel; under the large (50%) strain, G'' overwhelms G', inferring the conversion from gel to sol state. Excitingly, the G' and G'' of the hydrogel are approximately fully recovered within 30 s, and the recovery behavior is repeatable for many cycles, featuring a desired rapid self-healing property.

The excellent mechanical property and its rapid recovery ability of the folate/Zn^{2+} hydrogel make them excellent printable materials. Upon filling the viscous pregel into a syringe, various complicated 3D structures can be fabricated via simple injection. Figure 5 demonstrates the resultant diverse shapes such as numbers, characters, triangle, pyramid, hollow triangle, hollow cube, even heart.

Because both folate and Zn^{2+} are biocompatible, we investigate the potential to utilize the folate/Zn^{2+} hydrogel as a biomaterial. Cytotoxicity measurements (Figure 6a) suggest that the cell viability is almost 100% after incubating the human retinal pigment epithelial (hRPE) cells in the presence of up to 10 mg mL^{-1} folate/Zn^{2+} hydrogel in a cell culture medium. This property makes folate/Zn^{2+} hydrogel an appealing biomaterial for medical applications, such as tissue engineering and regeneration, which involve the injection of a biomaterial into a damaged tissue within a living organism. As a primary test, cellular experiment is conducted to examine hydrogel as a scaffold in tissue engineering. hRPE cells are added into the Zn^{2+} solution, followed by thorough mixing with a folate solution. The resulting viscous folate/Zn^{2+} pregel containing hRPE cells is printed through a pipette tip onto a glass coverslip and gelation is completed within 20 min on glass coverslip (for detailed procedure, please refer to Experimental Section in the Supporting Information). Figure 6b shows a 3D stack of the hRPE cells in a hydrogel stained with calcium AM and ethidium homodimer-1 after 48 h culture. Calcium AM detects living cells and emits green fluorescence, whereas ethidium homodimer-1 detects dead cells and emits red fluorescence. This live/dead assay gives a viability of 98.4 ± 0.6% (mean ± standard deviation), indicating the negligible cytotoxicity of folate/Zn^{2+} as a scaffold for 3D cell culture.

To test the biological functions of the printed cells, we monitor the activity of single cells in the hydrogel. On staining the cell with LysoTracker Red, the intracellular acidic compartments (in red; Figure 6c, including lysosomes and large dense-cored vesicles) can be observed over time at high resolution. The organelle dynamics (Figure 6d) suggest that the imbedded hRPE cells are viable, which retain normal 3D morphology, and exhibit various cellular functions, including proton pump activity, metabolic turnover, and membrane trafficking.[51,52] Successful 3D cell culture in the hydrogel can also be made for HeLa cells (Figure S5), indicating that the hydrogel is mechanically strong to provide physical support for various types of imbedded cells. Most importantly, they are nontoxic and permeable for nutrients, which are desirable properties for the long-term cell culture and tissue regeneration.[51,53,54]

DOI: 10.1021/acsami.7b18155
ACS Appl. Mater. Interfaces 2018, 10, 4530−4539

Furthermore, the coordination-triggered robust folate/Zn^{2+} hydrogel can also act as an ideal carrier for Gd^{3+} and therapeutic drugs. Because Gd^{3+} can significantly shorten the T_1 mode relaxation of nearby water molecules,[55,56] the contrast between the areas with and without Gd^{3+} is greatly increased, which has been widely used in practical applications.[57−59] Figure 7a demonstrates that on doping Gd^{3+} into the hydrogel, the value of $1/T_1$ increases linearly with increasing concentration of Gd^{3+}. The slope for the increase is 3.12 mM^{-1} s^{-1} at 600 MHz, which is comparable with literature reports,[60−62] indicating the hydrogel indeed displays an MRI imaging ability. In vivo MRI experiments in Figure 7b,c reveal that the T_1-weighted MR images of HeLa xenograft nude mice display a clear contrast enhancement in the tumor area after the intratumor injection of Gd^{3+}−folate/Zn^{2+} hydrogels. In a similar way, chemical drugs can also be doped into the hydrogel. Figure S6 demonstrates that on doping capecitabine (Xeloda, an effective anticancer drug) into folate/Zn^{2+} hydrogels, an intratumor injection of drug-bearing hydrogel displays a positive inhibition effect on the tumor.

Finally, the stability of the hydrogels within the biological temperature range is tested considering their practical applications. We found that the gels remain stable as the temperature amounts to 55 °C (Figure S7), presumably due to the strong coordination interaction that extensively exists within and between the fibers, which are very stable upon increasing temperature. Different from van der Waals attractions that cross-links other physical hydrogels, the coordination interaction can be strengthened at elevated temperature,[63,64] validating the strategy that coordination-triggered hydrogels are very advantageous in constructing printable biomaterials.

3. CONCLUSIONS

In conclusion, we reported the formation of a novel supramolecular metallo-folate hydrogel with a robust mechanical property. This newly discovered hydrogel was formed by direct mixing of aqueous solutions. Detailed mechanism analysis reveals that the gel was formed by a sequence of steps: petrin rings on folate form tetramers through hydrogen bonding, tetramers stack into nanofibers by $\pi-\pi$ stacking, zinc ion cross-links the nanofibers into larger-scale fibrils, and formation of the network with further cross-linked fibrils. The obtained folate/Zn^{2+} hydrogel can be injected, and printed, into various 3D structures. Good biocompatibility of the hydrogel endows them with potential application as a biomaterial. We have shown its ability to support hRPE and HeLa cells three-dimensionally, and the potential as an ideal carrier for imaging agent (Gd^{3+}) and chemodrug. Overall, the printability and biocompatibility of the novel hydrogel allow us to utilize this novel material in various technological applications. We expect that this coordination-triggered hierarchical self-assembly of small molecules may open up a new avenue for printable hydrogels.

■ ASSOCIATED CONTENT

Supporting Information

The Supporting Information is available free of charge on the ACS Publications website at DOI: 10.1021/acsami.7b18155.

Experimental section includes materials, gel preparation, structural characterizations, rheological measurement, printing procedure, cell experiments, animal experiments, and T_1 measurements; supporting figures include CD spectra and optical photos of folate solution with various amount of KNO_3 (Figure S1), UV−vis spectra of hydrogel with various molar ratios (Figure S2), small-angle X-ray scattering patterns of lyophilized hydrogel and in situ XRD pattern of hydrogel (Figure S3), stress-dependent and frequency-dependent oscillatory profiles of hydrogel with varied folate concentration (Figure S4), cell viability of hydrogel toward HeLa cells and 3D stacking of CLSM image of HeLa cells embedded hydrogel in live/dead assay (Figure S5), in vivo antitumor activity evaluation using capecitabine-doped folate/Zn^{2+} hydrogels (Figure S6), stress-dependent and frequency-dependent oscillatory profiles of hydrogel at different temperatures (Figure S7) (PDF)

■ AUTHOR INFORMATION

Corresponding Author

*E-mail: yunyan@pku.edu.cn.

ORCID

Yun Yan: 0000-0001-8759-3918

Notes

The authors declare no competing financial interest.

■ ACKNOWLEDGMENTS

The authors are grateful to National Natural Science Foundation of China (Grant No. 21573011, 21422302) and the Beijing National Laboratory for Molecular Sciences (BNLMS) for financial support.

■ REFERENCES

(1) Guvendiren, M.; Lu, H. D.; Burdick, J. A. Shear-Thinning Hydrogels for Biomedical Applications. *Soft Matter* **2012**, *8*, 260−272.

(2) Jungst, T.; Smolan, W.; Schacht, K.; Scheibel, T.; Groll, J. Strategies and Molecular Design Criteria for 3D Printable Hydrogels. *Chem. Rev.* **2016**, *116*, 1496−1539.

(3) Yu, L.; Ding, J. Injectable Hydrogels as Unique Biomedical Materials. *Chem. Soc. Rev.* **2008**, *37*, 1473−1481.

(4) Xing, R.; Liu, K.; Jiao, T.; Zhang, N.; Ma, K.; Zhang, R.; Zou, Q.; Ma, G.; Yan, X. An Injectable Self-Assembling Collagen−Gold Hybrid Hydrogel for Combinatorial Antitumor Photothermal/Photodynamic Therapy. *Adv. Mater.* **2016**, *28*, 3669−3676.

(5) Li, Y.; Wang, F.; Cui, H. Peptide-Based Supramolecular Hydrogels for Delivery of Biologics. *Bioeng. Transl. Med.* **2016**, *1*, 306−322.

(6) Hoare, T. R.; Kohane, D. S. Hydrogels in Drug Delivery: Progress and Challenges. *Polymer* **2008**, *49*, 1993−2007.

(7) Li, J. Y.; Mooney, D. J. Designing Hydrogels for Controlled Drug Delivery. *Nat. Rev. Mater.* **2016**, *1*, No. 16071.

(8) Wang, H.; Heilshorn, S. C. Adaptable Hydrogel Networks with Reversible Linkages for Tissue Engineering. *Adv. Mater.* **2015**, *27*, 3717−3736.

(9) Purcell, B. P.; Lobb, D.; Charati, M. B.; Dorsey, S. M.; Wade, R. J.; Zellars, K. N.; Doviak, H.; Pettaway, S.; Logdon, C. B.; Shuman, J. A.; Freels, P. D.; Gorman, J. H., 3rd; Gorman, R. C.; Spinale, F. G.; Burdick, J. A. Injectable and Bioresponsive Hydrogels for On-Demand Matrix Metalloproteinase Inhibition. *Nat. Mater.* **2014**, *13*, 653−661.

(10) Peak, C. W.; Nagar, S.; Watts, R. D.; Schmidt, G. Robust and Degradable Hydrogels from Poly(ethylene glycol) and Semi-Interpenetrating Collagen. *Macromolecules* **2014**, *47*, 6408−6417.

(11) Koshy, S. T.; Ferrante, T. C.; Lewin, S. A.; Mooney, D. J. Injectable, Porous, and Cell-Responsive Gelatin Cryogels. *Biomaterials* **2014**, *35*, 2477−2487.

(12) Su, D.; Jiang, L.; Chen, X.; Dong, J.; Shao, Z. Enhancing the Gelation and Bioactivity of Injectable Silk Fibroin Hydrogel with

DOI: 10.1021/acsami.7b18155
ACS Appl. Mater. Interfaces 2018, 10, 4530−4539

Laponite Nanoplatelets. *ACS Appl. Mater. Interfaces* **2016**, *8*, 9619−9628.
(13) Kundu, B.; Rajkhowa, R.; Kundu, S. C.; Wang, X. Silk Fibroin Biomaterials for Tissue Regenerations. *Adv. Drug Delivery Rev.* **2013**, *65*, 457−470.
(14) Yan, C.; Altunbas, A.; Yucel, T.; Nagarkar, R. P.; Schneider, J. P.; Pochan, D. J. Injectable Solid Hydrogel: Mechanism of Shear-Thinning and Immediate Recovery of Injectable Beta-Hairpin Peptide Hydrogels. *Soft Matter* **2010**, *6*, 5143−5156.
(15) Yan, C.; Pochan, D. J. Rheological Properties of Peptide-Based Hydrogels for Biomedical and Other Applications. *Chem. Soc. Rev.* **2010**, *39*, 3528−3540.
(16) Jonker, A. M.; Lowik, D. W. P. M.; van Hest, J. C. M. Peptide- and Protein-Based Hydrogels. *Chem. Mater.* **2012**, *24*, 759−773.
(17) Francis Suh, J. K.; Matthew, H. W. T. Application of Chitosan-Based Polysaccharide Biomaterials in Cartilage Tissue Engineering: A Review. *Biomaterials* **2000**, *21*, 2589−2598.
(18) Tan, H.; Chu, C. R.; Payne, K. A.; Marra, K. G. Injectable In Situ Forming Biodegradable Chitosan-Hyaluronic Acid Based Hydrogels for Cartilage Tissue Engineering. *Biomaterials* **2009**, *30*, 2499−2506.
(19) Peters, G. M.; Davis, J. T. Supramolecular Gels Made from Nucleobase, Nucleoside and Nucleotide Analogs. *Chem. Soc. Rev.* **2016**, *45*, 3188−3206.
(20) Rahim, M.; Björnmalm, M.; Suma, T.; Faria, M.; Ju, Y.; Kempe, K.; Müllner, M.; Ejima, H.; Stickland, A. D.; Caruso, F. Metal−Phenolic Supramolecular Gelation. *Angew. Chem., Int. Ed.* **2016**, *55*, 13803−13807.
(21) McMillan, R. A.; Conticello, V. P. Synthesis and Characterization of Elastin-Mimetic Protein Gels Derived from A Well-Defined Polypeptide Precursor. *Macromolecules* **2000**, *33*, 4809−4821.
(22) Rizzi, S. C.; Hubbell, J. A. Recombinant Protein-co-PEG Networks as Cell-Adhesive and Proteolytically Degradable Hydrogel Matrixes. Part I: Development and Physicochemical Characteristics. *Biomacromolecules* **2005**, *6*, 1226−1238.
(23) Chevallay, B.; Abdul-Malak, N.; Herbage, D. Mouse Fibroblasts in Long-Term Culture within Collagen Three-Dimensional Scaffolds: Influence of Crosslinking with Diphenylphosphorylazide on Matrix Reorganization, Growth, and Biosynthetic and Proteolytic Activities. *J. Biomed. Mater. Res.* **2000**, *49*, 448−459.
(24) Rault, I.; Frei, V.; Herbage, D.; Abdul-Malak, N.; Huc, A. Evaluation of Different Chemical Methods for Cross-linking Collagen Gel, Films and Sponges. *J. Mater. Sci.: Mater. Med.* **1996**, *7*, 215−221.
(25) Maitra, J.; Shukla, V. K. Cross-Linking in Hydrogels-A Review. *Am. J. Polym. Sci.* **2014**, *4*, 25−31.
(26) Appel, E. A.; Tibbitt, M. W.; Webber, M. J.; Mattix, B. A.; Veiseh, O.; Langer, R. Self-Assembled Hydrogels Utilizing Polymer−Nanoparticle Interactions. *Nat. Commun.* **2015**, *6*, No. 6295.
(27) Tseng, T. C.; Tao, L.; Hsieh, F. Y.; Wei, Y.; Chiu, I. M.; Hsu, S. H. An Injectable, Self-Healing Hydrogel to Repair the Central Nervous System. *Adv. Mater.* **2015**, *27*, 3518−3524.
(28) Ejima, H.; Richardson, J. J.; Liang, K.; Best, J. P.; van Koeverden, M. P.; Such, G. K.; Cui, J.; Caruso, F. One-Step Assembly of Coordination Complexes for Versatile Film and Particle Engineering. *Science* **2013**, *341*, 154−157.
(29) Chaudhuri, O.; Gu, L.; Klumpers, D.; Darnell, M.; Bencherif, S. A.; Weaver, J. C.; Huebsch, N.; Lee, H. P.; Lippens, E.; Duda, G. N.; Mooney, D. J. Hydrogels with Tunable Stress Relaxation Regulate Stem Cell Fate and Activity. *Nat. Mater.* **2016**, *15*, 326−334.
(30) Grindy, S. C.; Holten-Andersen, N. Bio-Inspired Metal-Coordinate Hydrogels with Programmable Viscoelastic Material Functions Controlled by Longwave UV Light. *Soft Matter* **2017**, *13*, 4057−4065.
(31) Shi, L. Y.; Wang, F. L.; Zhu, W.; Xu, Z. P.; Fuchs, S.; Hilborn, J.; Zhu, L. J.; Ma, Q.; Wang, Y. J.; Weng, X. S.; Ossipov, D. A. Self-Healing Silk Fibroin-Based Hydrogel for Bone Regeneration: Dynamic Metal-Ligand Self-Assembly Approach. *Adv. Funct. Mater.* **2017**, *27*, No. 1700591.
(32) Faul, C. F. J.; Antonietti, M. Ionic Self-Assembly: Facile Synthesis of Supramolecular Materials. *Adv. Mater.* **2003**, *15*, 673−683.
(33) Institute of Medicine (US) Standing Committee on the Scientific Evaluation of Dietary Reference Intakes. *Dietary Reference Intakes for Thiamin, Riboflavin, Niacin, Vitamin B6, Folate, Vitamin B12, Pantothenic Acid, Biotin, and Choline*; National Academies Press, 1998.
(34) Shils, M. E.; Shike, M. *Modern Nutrition in Health and Disease*; Lippincott Williams & Wilkins, 2006.
(35) Bailey, L.; Moyers, S.; Gregory, J.; Bowman, B.; Russell, R. *Present Knowledge in Nutrition*; International Life Sciences Institute: Washington, DC, 2001.
(36) Lokesh; Suryaprakash, N. Self-Assembly of Folic Acid: A Chiral-Aligning Medium for Enantiodiscrimination of Organic Molecules in An Aqueous Environment. *Chem. - Eur. J.* **2012**, *18*, 11560−11563.
(37) Bonazzi, S.; Demorais, M. M.; Gottarelli, G.; Mariani, P.; Spada, G. P. Self-Assembly and Liquid-Crystal Formation of Folic-Acid Salts. *Angew. Chem., Int. Ed.* **1993**, *32*, 248−250.
(38) Ciuchi, F.; Dinicola, G.; Franz, H.; Gottarelli, G.; Mariani, P.; Bossi, M. G. P.; Spada, G. P. Self-Recognition and Self-Assembly of Folic-Acid Salts - Columnar Liquid-Crystalline Polymorphism and the Column Growth-Process. *J. Am. Chem. Soc.* **1994**, *116*, 7064−7071.
(39) Kato, T.; Matsuoka, T.; Nishii, M.; Kamikawa, Y.; Kanie, K.; Nishimura, T.; Yashima, E.; Ujiie, S. Supramolecular Chirality of Thermotropic Liquid-Crystalline Folic Acid Derivatives. *Angew. Chem., Int. Ed.* **2004**, *43*, 1969−1972.
(40) Chakraborty, P.; Roy, B.; Bairi, P.; Nandi, A. K. Improved Mechanical and Photophysical Properties of Chitosan Incorporated Folic Acid Gel Possessing the Characteristics of Dye and Metal Ion Absorption. *J. Mater. Chem.* **2012**, *22*, 20291−20298.
(41) Xing, P.; Chu, X.; Ma, M.; Li, S.; Hao, A. Supramolecular Gel from Folic Acid with Multiple Responsiveness, Rapid Self-Recovery and Orthogonal Self-Assemblies. *Phys. Chem. Chem. Phys.* **2014**, *16*, 8346−8359.
(42) Gottarelli, G.; Lena, S.; Masiero, S.; Pieraccini, S.; Spada, G. P. The Use of Circular Dichroism Spectroscopy for Studying the Chiral Molecular Self-Assembly: An Overview. *Chirality* **2008**, *20*, 471−485.
(43) Gao, X. D.; Wang, Y. J.; Wang, X. L.; Guo, X. F.; Huang, J. B.; Yan, Y. Concentration-Tailored Self-Assembly Composition and Function of the Coordinating Self-Assembly of Perylenetetracarboxylate. *J. Mater. Chem. C* **2017**, *5*, 8936−8943.
(44) Tsukruk, V.; Shilov, V. *Striktura polimernykh zhidkikh kristallov (Structure of Polymeric Liquid Crystals)*; Naukova Dumka: Kiev, USSR, 1990.
(45) Deacon, G. B.; Phillips, R. J. Relationships between the Carbon-Oxygen Stretching Frequencies of Carboxylato Complexes and the Type of Carboxylate Coordination. *Coord. Chem. Rev.* **1980**, *33*, 227−250.
(46) Qiao, Y.; Lin, Y.; Wang, Y.; Yang, Z.; Liu, J.; Zhou, J.; Yan, Y.; Huang, J. Metal-Driven Hierarchical Self-Assembled One-Dimensional Nanohelices. *Nano Lett.* **2009**, *9*, 4500−4504.
(47) Nakamoto, K. *Infrared and Raman Spectra of Inorganic and Coordination Chemistry Part A: Theory and Applications in Inorganic Chemistry*, 5th ed.; Wiley: New York, 1997.
(48) Kaucher, M. S.; Lam, Y. F.; Pieraccini, S.; Gottarelli, G.; Davis, J. T. Using Diffusion NMR to Characterize Guanosine Self-Association: Insights into Structure and Mechanism. *Chemistry* **2004**, *11*, 164−173.
(49) Ueda, J. I.; Hanaki, A.; Yoshida, N.; Nakajima, T. Complex-Formation of Zinc(Ii) Ion with Glycylglycyl-L-Histidine - an Investigation by Proton Nuclear-Magnetic-Resonance Spectroscopy. *Chem. Pharm. Bull.* **1986**, *34*, 1315−1318.
(50) Gong, J. P. Why Are Double Network Hydrogels So Tough? *Soft Matter* **2010**, *6*, 2583−2590.
(51) Li, C.; Faulkner-Jones, A.; Dun, A. R.; Jin, J.; Chen, P.; Xing, Y.; Yang, Z.; Li, Z.; Shu, W.; Liu, D.; et al. Rapid Formation of a Supramolecular Polypeptide−DNA Hydrogel for In Situ Three-Dimensional Multilayer Bioprinting. *Angew. Chem., Int. Ed.* **2015**, *54*, 3957−3961.
(52) Yang, L.; Dun, A. R.; Martin, K. J.; Qiu, Z.; Dunn, A.; Lord, G. J.; Lu, W.; Duncan, R. R.; Rickman, C. Secretory Vesicles Are

DOI: 10.1021/acsami.7b18155
ACS Appl. Mater. Interfaces 2018, 10, 4530−4539

Preferentially Targeted to Areas of Low Molecular SNARE Density. *PLoS One* **2012**, *7*, No. e49514.
(53) Wei, Q.; Xu, M.; Liao, C.; Wu, Q.; Liu, M.; Zhang, Y.; Wu, C.; Cheng, L.; Wang, Q. Printable Hybrid Hydrogel by Dual Enzymatic Polymerization with Superactivity. *Chem. Sci.* **2016**, *7*, 2748−2752.
(54) Wu, C.; Fan, W.; Zhou, Y.; Luo, Y.; Gelinsky, M.; Chang, J.; Xiao, Y. 3D-printing of Highly Uniform $CaSiO_3$ Ceramic Scaffolds: Preparation, Characterization and in vivo Osteogenesis. *J. Mater. Chem.* **2012**, *22*, 12288−12295.
(55) Bruckman, M. A.; Yu, X.; Steinmetz, N. F. Engineering Gd-Loaded Nanoparticles to Enhance MRI Sensitivity via T1 Shortening. *Nanotechnology* **2013**, *24*, No. 462001.
(56) Villaraza, A. J. L.; Bumb, A.; Brechbiel, M. W. Macromolecules, Dendrimers, and Nanomaterials in Magnetic Resonance Imaging: the Interplay between Size, Function, and Pharmacokinetics. *Chem. Rev.* **2010**, *110*, 2921−2959.
(57) Wang, J.; As, H.; Keizer, A.; Cohen Stuart, M. A.; der Gucht, J.; et al. Controlled Mixing of Lanthanide (III) Ions in Coacervate Core Micelles. *Chem. Commun.* **2013**, *49*, 3736−3738.
(58) Colombo, M.; Carregal-Romero, S.; Casula, M. F.; Gutierrez, L.; Morales, M. P.; Bohm, I. B.; Heverhagen, J. T.; Prosperi, D.; Parak, W. J. Biological Applications of Magnetic Nanoparticles. *Chem. Soc. Rev.* **2012**, *41*, 4306−4334.
(59) Torres, S.; Martins, J. A.; André, J. P.; Geraldes, C. F.; Merbach, A. E.; Tóth, É. Supramolecular Assembly of An Amphiphilic GdIII Chelate: Tuning the Reorientational Correlation Time and the Water Exchange Rate. *Chem. - Eur. J.* **2006**, *12*, 940−948.
(60) Castelli, D. D.; Gianolio, E.; Crich, S. G.; Terreno, E.; Aime, S. Metal Containing Nanosized Systems for MR-Molecular Imaging Applications. *Coord. Chem. Rev.* **2008**, *252*, 2424−2443.
(61) Wu, Z.; Huang, J.; Yan, Y. Electrostatic Polyion Micelles with Fluorescence and MRI Dual Functions. *Langmuir* **2015**, *31*, 7926−7933.
(62) Harrison, V. S.; Carney, C. E.; MacRenaris, K. W.; Waters, E. A.; Meade, T. J. Multimeric Near IR−MR Contrast Agent for Multimodal In Vivo Imaging. *J. Am. Chem. Soc.* **2015**, *137*, 9108−9116.
(63) Qiao, Y.; Lin, Y.; Yang, Z.; Chen, H.; Zhang, S.; Yan, Y.; Huang, J. Unique Temperature-Dependent Supramolecular Self-Assembly: From Hierarchical 1D Nanostructures to Super Hydrogel. *J. Phys. Chem. B* **2010**, *114*, 11725−11730.
(64) Wang, Y.; Gao, X.; Xiao, Y.; Zhao, Q.; Yang, J.; Yan, Y.; Huang, J. Temperature Dependent Coordinating Self-Assembly. *Soft Matter* **2015**, *11*, 2806−2811.

DOI: 10.1021/acsami.7b18155
ACS Appl. Mater. Interfaces 2018, 10, 4530−4539